



Multipoint chord reference system for track irregularity: Part II – Numerical analysis



Yuan Wang^{a,b,d}, Huiyue Tang^{c,d}, Ping Wang^{a,b}, Xiang Liu^d, Rong Chen^{a,b,*}

^a School of Civil Engineering, Southwest Jiaotong University, Chengdu, China

^b Key Laboratory of High-Speed Railway Engineering, Ministry of Education, Chengdu, China

^c School of Electrical Engineering, Southwest Jiaotong University, Chengdu, China

^d Department of Civil and Environmental Engineering, Rutgers, The State University of New Jersey, NJ, USA

ARTICLE INFO

Article history:

Received 23 June 2018

Received in revised form 23 January 2019

Accepted 26 January 2019

Available online 2 February 2019

Keywords:

Multipoint chord reference system

Transfer function

Numerical simulation

Fourier transform

Track geometry irregularity

ABSTRACT

This paper proposed a novel approach to measure track irregularity by using a multipoint chord reference (MCR) system. In Part I of this study, the theory and methodology were introduced and the performance in the spatial domain were analyzed through theoretical proofs. The current paper analyzes the performance of an MCR system in the wavelength domain based on numerical approaches regarding two aspects: transfer function (TF) and false track geometry (FTG) in wavelength domain (FWD). To address the short wavelength performance of an MCR system, the minimum measurable wavelength (MMW) was analyzed according to the TF of different MCR systems. The numerical results are consistent with the theoretical value of MMW. Numerical experiments based on Fourier transform were conducted to analyze the FWD for a given MCR system. Critical wavelength (CW) is proposed to quantify the long wavelength performance. Moreover, the influences of the order, configuration, and length of rail on the performance of FWD are considered for different MCR systems. The main results suggest that (1) a higher order leads to better system performance in the wavelength domain, smaller MMW, and larger CW. (2) In addition, the sparse configurations have a significant influence on the FTG for the short wavelengths below 1.5 m. (3) The magnitude of FTG increases rapidly with 1.91 power of the wavelength. (4) The magnitude of FTG for a long wavelength increases with 1.5 power of the rail length, whereas those of short and intermediate wavelengths drop with -0.562 and -0.647 powers of rail length, respectively. (5) CW increases with the increasing order of the MCR system or with the increase in the length of rail to be measured. The MMW, FWD, and CW proposed in this paper are essential tools, which can be used to predict and optimize the performance of an MCR system.

© 2019 Published by Elsevier Ltd.

1. Introduction

In Part I of this study, a unified framework of a multipoint chord reference system (MCR system) was introduced with definitions on n -ordered MCR(n) systems, standard sampling interval (SSI), MCR (n, m) system, minimum measurable wavelength (MMW), and stability. Mathematical models were established based on sensor fusion and least square optimization techniques. The error property in spatial domain was studied using the error amplification factor (EAF), which can be used to quantify the error accumulation characteristics of MCR systems. Table 1 describes the terminologies, variables, and operators used in this paper.

The current paper focuses on the performance of MCR systems in the wavelength domain. The main methodology used in this study is based on numerical simulation. We used all the definitions, terminologies, and symbols of an MCR system as stated in the previous paper (Part I). Note that the whole framework of an MCR system is newly established, the error accumulation characteristics in wavelength domain are completely blank, except for those used in our previous publication [1] in which we studied the error theory of the mid-chord offset (MCO) system, a special case of MCR(1, 1) system, in both spatial and wavelength domains.

In this study, the performance of an MCR system in the wavelength domain was analyzed based on two aspects: transfer function (TF) and false track geometry (FTG) in wavelength domain (FWD).

TF is widely used to study the performance of various rail-irregularity-measurement techniques, such as the inertial reference method [2,3], MCO system [1,4–6] or other chord-based

* Corresponding author at: School of Civil Engineering, Southwest Jiaotong University, Chengdu, China.

E-mail address: chenrong@home.swjtu.edu.cn (R. Chen).

Table 1
Terminologies, variables, and operators.

Terminology	Explanation
MCR system	Multipoint chord reference system
MCO system	Mid-chord offset method
SSI	Standard sampling interval
EP	Equidistance point that divides a chord by equal length segmentations
ith-EP	The <i>i</i> th equidistance point that divides a chord by ratio of <i>i</i> : (<i>n</i> + 1 – <i>i</i>)
FTG	False track geometry
MMW	Minimum measurable wavelength
EAF	Error amplification factor
FWD	False track geometry in wavelength domain
CW	Critical wavelength
PSD	Power spectral density
Variable	Denotation
<i>l, L</i>	Lengths of track section and reference chord, respectively.
<i>n</i>	Order of an MCR(<i>n</i>) system.
ΔL_s	= $L/(n + 1)$, standard sampling interval (SSI) of an MCR(<i>n</i>) system.
<i>k</i>	= $\{k_i i = 0, 1, \dots, m; k_i \in N^+ \cap [1, n]\}$, an increasing sequence that specifies the configuration of an MCR(<i>n</i>) system.
<i>N</i>	= $(n + 1) \cdot l/L + 1$; the number of discretized segments of a rail section by SSI.
y	= $(y_0, y_1, \dots, y_N)^T$; discretization of $f(x)$.
J_k	Matrix with size $m \times n$ with $J_k(i, j) = \begin{cases} 1, j = k_i \\ 0, j \neq k_i \end{cases}$
λ_i	= $i/(n + 1) - 1$; ratio of two parts divided by the <i>i</i> th EP.
$\bar{\lambda}_i$	= $-1 - \lambda_i = -i/(n + 1)$.
M	= $[\lambda I - (1 - \lambda)]$ with $\lambda = (\lambda_1, \lambda_1, \dots, \lambda_n)^T$, the measurement matrix of the MCR system.
M_k	= $[\lambda_k \ J_k \ -(1 + \lambda_k)]$; the measurement matrix.
A_{k_i}	= $\begin{bmatrix} \lambda_{k_1} & 0 & \dots & 1 & \dots & 0 & \bar{\lambda}_{k_1} \\ & \lambda_{k_2} & 0 & \dots & 1 & \dots & 0 & \bar{\lambda}_{k_2} \\ & & \ddots & & & & & \ddots \\ & & & \lambda_{k_i} & 0 & \dots & 1 & \dots & 0 & \bar{\lambda}_{k_i} \end{bmatrix}$, each row containing the <i>i</i> th row of M_k .
H	= $[\mathbf{h}_0, \mathbf{h}_1, \dots, \mathbf{h}_{N-n-1}]$; the integrated measured chord versine matrix.
F(y)	= $[\mathbf{y}_0, \mathbf{y}_1, \dots, \mathbf{y}_{N-n-1}]$; the matrix contains the track geometry to be measured.
$\bar{\mathbf{H}}$ and $\bar{\mathbf{H}}_k$	The measured chord versine matrix containing measurement error
E and E_k	Measurement error matrix.
$\bar{\mathbf{h}}_i$	= $\{\bar{h}_{i,0}, \bar{h}_{i,1}, \dots, \bar{h}_{i,N-n-1}\}^T$ is the transpose of the <i>i</i> th row of $\bar{\mathbf{H}}$.
y*	= $\mathcal{A}_M(\mathbf{H} + \mathbf{E})$; the least square estimation of y .
y	= $\mathbf{y} - \mathbf{y}^* = \mathcal{A}_M(\mathbf{E})$; the false track geometry (FTG).
Y and Y*	The Fourier transform of discretized rail irregularity sequences y and y*
<i>w</i>	Represents wavelength coordinate, generally used as subscript.
<i>p</i>	Represents spatial coordinate, generally used as subscript.
Y_w and Y*_w	The values of Y and Y* at given wavelength <i>w</i> .
Y	The FTG in wavelength domain.
Y_w	The value of Y at given wavelength <i>w</i> .
T	= $\text{Abs}(\frac{Y}{Y^*})$; the transfer function.
P* and P	Are the power spectrum densities (PSDs) of y and y* .
A_w	= $\text{Amp}(Y_w)$
θ_w	= $\text{Ang}(Y_w)$
A_{max}	= $\text{Max}_{w \geq l} (A_w)$
A_{min}	= $\text{Mean}_{w < 1.5L} (A_w)$
A_{mid} and P	The two parameters of power exponent function for the description of the intermediate wavelengths
W_c	Critical wavelength
$f_{wd}(w, \mathbf{M}_k, l, L)$	FWD function with respect to <i>w, M_{k, l}</i> , and <i>L</i> .
Operator	Denotation
E (·)	Mathematical expectation of a random variable.
Var (·)	Variance of a random variable.
Mean (·)	Mean value of a vector or sequence.
Std (·)	Standard deviation of a vector or sequence.
Max (·)	Maximal value of a vector or sequence.
Amp (·)	Modulus of complex number.
Ang (·)	Angle of complex number.
A_M (X)	= $(\sum_{i=1}^n \mathbf{A}_i^T \mathbf{A}_i)^{-1} \cdot \sum_{i=1}^n \mathbf{A}_i^T (\mathbf{x}'_i)$; the restoration operator of MCR system, where \mathbf{x}'_i is the transpose of the <i>i</i> th row of matrix X .

methods [7–9]. In general, TF of a measurement system is defined in the wavelength domain. TF = 1 indicates a good performance. When TF at some wavelength is less or larger than 1, the measured magnitude at that wavelength is reduced or enlarged, respectively.

In particular, TF = 0 at some wavelength implies that the waveform at that wavelength cannot be measured.

FTG [1] refers to the measurement error term generated from the noise of sensors during the restoration process of an MCR

system. When not counting the sensor error, the magnitude of FTG is zero, indicating that the measurement result is absolutely accurate. When the sensor error is considered, the characteristics of FWD are key for analyzing the performance of an MCR system in the wavelength domain.

The contributions of the current paper are summarized as follows.

A numerical experiment of the measurement process is proposed in Section 4 to estimate the transfer function of a given MCR system.

A numerical experiment based on Fourier transform is introduced in Section 5.2 to analyze FWD.

The FWD function containing four parameters is proposed in Section 5.3 to describe the FWD.

The critical wavelength (CW) is defined in Section 5.4 to quantify the performance the MCR system.

The influence of the major factors on the performance of FWD for different MCR systems are analyzed in Section 6.

2. Fundamentals of an MCR system

2.1. Brief introduction to an MCR system

This section gives a brief introduction on MCR systems. The measurement principle of an n -ordered MCR system is illustrated in Fig. 1. A chord formed between two points on the rail, represented as the straight line \overline{AC} , behaves as a reference, and the read-out of each sensor at the related EP of the chord is the distance (on normal direction) between the EP and rail to be measured. Table 1 describes the terminologies, variables, and operators used in this paper.

Some main concepts of an MCR system are presented as follows. For more details, please refer to Part I paper.

MCR(n) with order n : As illustrated in Fig. 1, an n -ordered MCR is defined as a chord-based measurement system with all sensors mounted at the EPs of a chord. The i th EP is the point dividing the chord at a ratio of $i : (n + 1 - i)$.

SSI of MCR(n): the SSI is defined as

$$\Delta L_s = \frac{1}{n + 1} \cdot L, \tag{1}$$

where L is the length of the reference chord. It indicates that for a higher order of MCR(n), the SSI ΔL_s is smaller (the sampling frequency is higher). Furthermore, in this study, the high- and low-frequency samplings were considered if the sampling intervals were $\Delta L < \Delta L_s$ and $\Delta L > \Delta L_s$, respectively.

MCR(n, m) system: An MCR(n, m) is defined as an n -ordered MCR system with m sensors mounted on the EPs of a chord. n represents the order and m represents the number of sensors. The configuration of the sensor layout (hereafter termed as configuration) is specified by an increasing sequence $k = \{k_i | i = 0, 1, \dots, m; k_i \in N^+ \cap [1, n]\}$.

MMW: the MMW is defined as the minimal wavelength that can be measured through an MCR system. For an MCR(n) system with full configuration, the MMW is $2L/(n + 1)$ for the sampling interval of $\Delta L \leq \Delta L_s$.

2.2. Measurement model

The measurement model of an MCR(n, m) system with configuration specified by k is given as

$$\bar{\mathbf{H}}_k = \mathbf{M}_k \cdot \mathbf{F}(\mathbf{y}) + \mathbf{E}, \tag{2}$$

where $\mathbf{y} = (y_0, y_1, \dots, y_N)^T$ is the discretized sequence of rail irregularity to be measured and $N = l/\Delta L_s$. $\bar{\mathbf{H}}_k$ is the measured chord versine matrix and $\mathbf{F}(\mathbf{y})$ is a matrix generated by \mathbf{y} and is given as

$$\mathbf{F}(\mathbf{y}) = \begin{bmatrix} y_0 & y_1 & \dots & y_{N-n-1} \\ y_1 & y_2 & \dots & y_{N-n} \\ \vdots & \vdots & \dots & \vdots \\ y_{n+1} & y_{n+2} & \dots & y_N \end{bmatrix} \tag{3}$$

\mathbf{M}_k is the measurement matrix given as

$$\mathbf{M}_k = [\lambda_k \quad \mathbf{J}_k \quad -(1 + \lambda_k)], \tag{4}$$

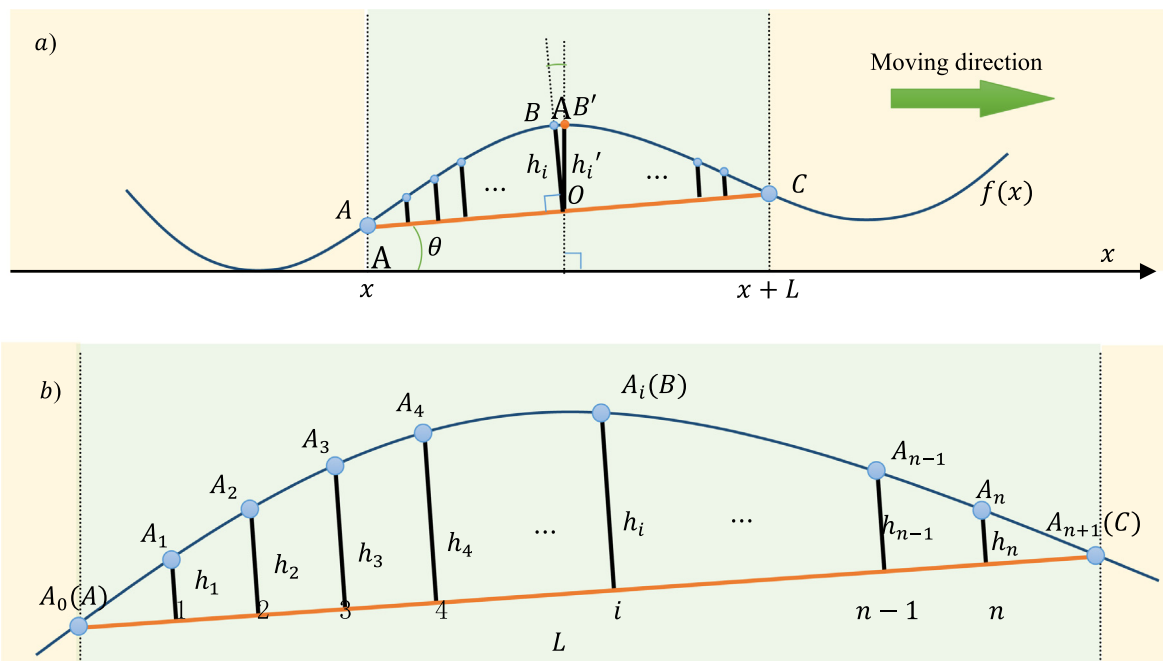


Fig. 1. Measurement principle of the MCR system with order n . A chord length of L is divided into $n + 1$ equal length segments, and the sensors are mounted as the EPs.

where $\lambda_k = (\lambda_{k_1}, \lambda_{k_2}, \dots, \lambda_{k_m})$ with

$$\lambda_{k_i} = \frac{k_i}{n+1} - 1, \quad (5)$$

and \mathbf{J}_k is a matrix of size $m \times n$:

$$\mathbf{J}_k(i, j) = \begin{cases} 1, & j = k_i; \\ 0, & j \neq k_i \end{cases}; i = 1, \dots, m; j = 1, \dots, n. \quad (6)$$

2.3. Restoration model

Given an MCR(n, m) system with measurement matrix specified by \mathbf{M}_k , the restoration of the original waveform can be achieved from the measured chord versine matrix $\bar{\mathbf{H}}_k$ by using the following model:

$$\mathbf{y}^* = \mathcal{A}_{\mathbf{M}_k}(\bar{\mathbf{H}}_k) = \left(\sum_{i=1}^m \mathbf{A}_{k_i}^T \mathbf{A}_{k_i} \right)^{-1} \cdot \sum_{i=1}^m \mathbf{A}_{k_i}^T (\bar{\mathbf{h}}_{k_i}^T), \quad (7)$$

where $\bar{\mathbf{h}}_{k_i}^T$ is the transpose of the i th row of the measured chord versine matrix $\bar{\mathbf{H}}$, and

$$\mathbf{A}_{k_i} = \begin{bmatrix} \lambda_{k_i} & 0 & \dots & 1 & \dots & 0 & \bar{\lambda}_{k_i} \\ & \lambda_{k_i} & 0 & \dots & 1 & \dots & 0 & \bar{\lambda}_{k_i} \\ & & \dots & & \dots & & & \dots \\ & & & \lambda_{k_i} & 0 & \dots & 1 & \dots & 0 & \bar{\lambda}_{k_i} \end{bmatrix}, \quad (8)$$

where $\bar{\lambda}_{k_i} = -1 - \lambda_{k_i}$. Each row of \mathbf{A}_{k_i} contains the i th row of \mathbf{M}_k . If $\sum_{i=1}^m \mathbf{A}_{k_i}^T \mathbf{A}_{k_i}$ is not invertible, then the Moore–Penrose pseudo-inverse [10] is used.

3. Transfer function of the MCR system

3.1. Numerical simulation of the measurement process

A numerical simulation of the measurement process was designed and conducted, as illustrated in Fig. 2. The simulation process is detailed in Appendix A. The track geometry irregularity used in the simulation can be practically measured or numerically generated. In this study, the track-geometry irregularity was generated based on the sixth-grade track irregularity of the PSD of U.S. railways [11].

3.2. Restoration of the original waveform

The most important advantage of the simulation process is that the precision of sensors can be easily adjusted as required. As a result, the error accumulation property of the MCR system in the wavelength domain can be analyzed.

By simulating the measurement process proposed in Section 4.1, we can obtain the measured chord versine matrix, based on which the restoration model given in Section 3.3 is used to calculate the restored waveform, namely the final measurement result.

Consider a case in which a 500-m rail longitudinal profile is generated numerically; the profile is measured using the MCR (19) system with a 1-m-long chord. In this case, no sensor error is included, namely $E(e^2) = \sigma^2 = 0$. The results are illustrated in Fig. 3. As shown, the measured waveform is almost but not completely the same as the original waveform. The enlarged view of the waveform shows that some details regarding short wavelengths are lost. The loss of details is caused by the MMW of a given order MCR system. For the MCR(19) system, the MMW is $2L/(19+1) = 0.1$ m, implying that the MCR(19) system cannot measure the wavelengths below 0.1 m.

3.3. TF

The TF was used to analyze the property of MCR systems, and it is defined as

$$\mathbf{T} = \text{Amp} \left(\frac{\mathbf{Y}^*}{\mathbf{Y}} \right), \quad (10)$$

where $\text{Amp}(\cdot)$ is used to obtain modulus of a complex number; \mathbf{Y} and \mathbf{Y}^* denote the Fourier transforms of the discretized rail irregularity sequences \mathbf{y} and \mathbf{y}^* , respectively. \mathbf{y} and \mathbf{y}^* denote the original and MCR-measured rail irregularities. Y_w^* and Y_w at wavelength w are given as

$$Y_w^* = \sum_{p=0}^{N-1} y_p^* \cdot e^{-2\pi i \frac{p}{N} \frac{1}{w}} \quad (11)$$

$$Y_w = \sum_{p=0}^{N-1} y_p \cdot e^{-2\pi i \frac{p}{N} \frac{1}{w}}, \quad (12)$$

where p represents spatial coordinate along the rail and w represents wavelength relating to frequency domain. The relationship between \mathbf{y}^* and \mathbf{y} can be described as

$$\mathbf{y}^* = \mathcal{A}_{\mathbf{M}_k}(\mathbf{M}_k \cdot \mathbf{F}(\mathbf{y}) + \mathbf{E}) = \mathbf{y} + \mathcal{A}_{\mathbf{M}_k}(\mathbf{E}). \quad (13)$$

To ensure the significance of TF \mathbf{T} given in Eq. (10), an interpolation of \mathbf{y}^* is necessary to ensure it shares the same length and sampling interval of \mathbf{y} . A TF close to 1 indicates a good performance at the corresponding wavelength, and vice versa. Particularly, when TF closes to 0, the components around that wavelengths cannot be measured by the MCR system.

However, instead of estimating the TF according to the definition given in Eq. (10), this paper uses a lesser noisy approach as

$$\mathbf{T} = \sqrt{\frac{\mathbf{P}^*}{\mathbf{P}}}, \quad (14)$$

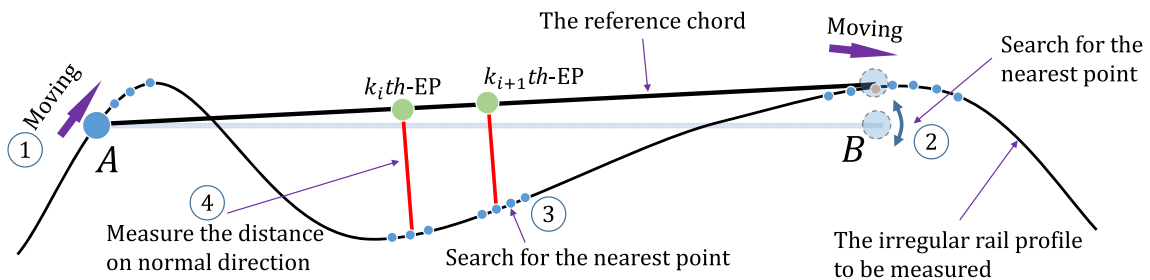


Fig. 2. Numerical simulation of the measurement process.

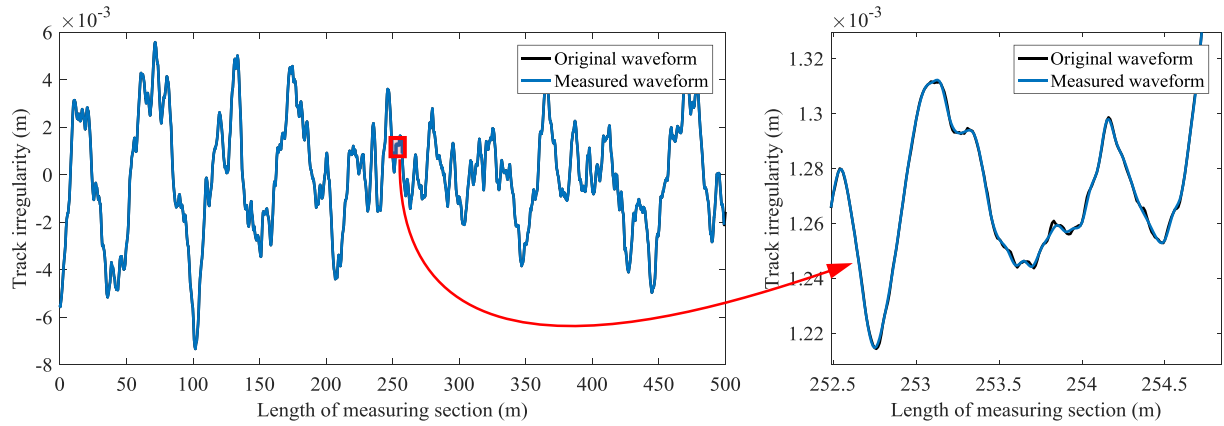


Fig. 3. Comparison between the original waveform and measured result using the MCR(19) system based on simulation.

where \mathbf{P}^* and \mathbf{P} are the PSDs of \mathbf{y} and \mathbf{y}^* , respectively, and are defined as

$$\mathbf{P}^* = \frac{1}{N} (\text{Amp}(\mathbf{Y}^*))^2; \mathbf{P} = \frac{1}{N} (\text{Amp}(\mathbf{Y}))^2. \quad (15)$$

Again, we will not use this definition for computation. Several methods exist for the estimation of PSD, for example, periodogram [12] and Welch's method [12,13]. In this paper, we used Burg's estimator [13].

3.4. TF of the MCR system with different orders

This section presents the analysis of the TF of the MCR system with different orders. Four MCR(n) systems were considered with orders $n=4, 9, 19,$ and 29 . The simulation results are illustrated in Fig. 4. The track-geometry irregularity waveform used in the simulation is the same as in the case illustrated in Fig. 3.

Fig. 4(a) shows the PSDs of the original and measured waveforms. Note that the fluctuation around the short wavelengths (less than 1 m) is affected by the interpolation of measured data to ensure its length is the same with that of the original waveform. Fig. 4(b) shows the TF of the four MCR systems. As shown, with the increasing orders of the MCR system, the TF shows a good performance around shorter wavelengths.

Moreover, the theoretical MMW and wavelengths (m) for $\text{TF} > 0.75$ are listed in Table 2. The simulated results are almost the same as the theoretical MMW except for a slight difference.

The TF performance shows that the measurement can be taken as absolutely accurate beyond the MMW when no sensor errors are considered. According to Eq. (13), the final measurement result is a

Table 2
The MMW and wavelengths when $\text{TF} = 0.75$.

MCR system	MMW (m)	Wavelengths (m) when $\text{TF} = 0.75$
MCR(4)	0.4	0.3948
MCR(9)	0.2	0.1974
MCR(19)	0.1	0.1063
MCR(29)	0.0667	0.0707

linear combination of the real value and an error term; thus, the remainder of the problem is how the error term performs in the wavelength domain.

4. FTG and FWD function

4.1. FWD

According to restoration model given in Section 3.3, the final measurement result \mathbf{y}^* is obtained as

$$\mathbf{y}^* = \mathcal{A}_M(\mathbf{H} + \mathbf{E}) = \mathbf{y} + \mathcal{A}_M(\mathbf{E}) = \mathbf{y} + \mathbf{y}. \quad (16)$$

Here, the measurement error or the error term mentioned in Section 4.3 is termed FTG $\mathbf{y} = (y_0, y_1, \dots, y_N)^T$, which is defined as

$$\mathbf{y} = \mathbf{y}^* - \mathbf{y}. \quad (17)$$

Assuming that we are measuring an absolute straight rail, the magnitude of the track irregularity is zero. As a result, the theoretical chord versine values are all zeros, that is, $\mathbf{H} = 0$. However, for a

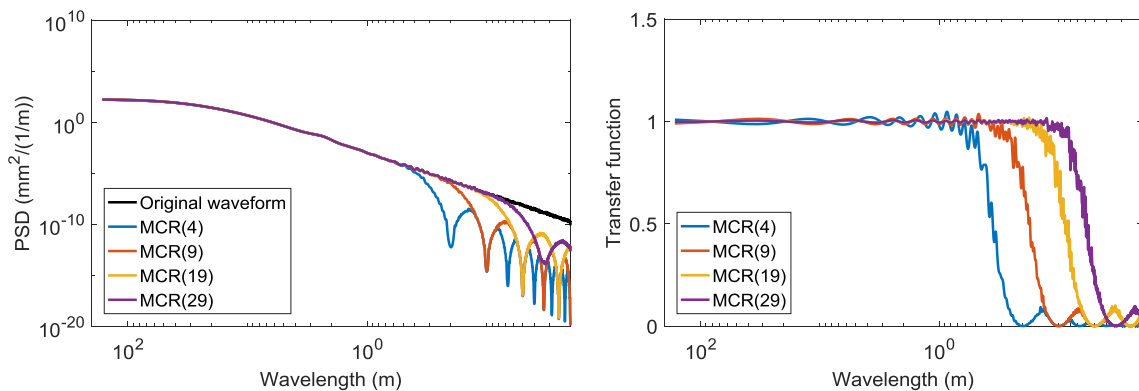


Fig. 4. Simulation result using MCR system with orders of 4, 9, 19, and 29. (a) PSDs of the original and measured waveforms. (b) TF of the MCR systems.

real measurement instrument, the sensors measure the chord versine values with a degree of uncertainty, $\mathbf{E} \neq 0$. Further, the real measured chord versine matrix is described as

$$\bar{\mathbf{H}} = \mathbf{H} + \mathbf{E} = \mathbf{E}. \quad (18)$$

Therefore,

$$\mathbf{y} = \mathcal{A}_M(\mathbf{E}). \quad (19)$$

In this study, we defined the EAF to analyze the error property in the spatial domain and analyze the FWD.

Given a matrix with sensor error as

$$\mathbf{E} = \begin{bmatrix} e_{1,0} & e_{1,1} & & e_{1,N-n-2} & e_{1,N-n-1} \\ e_{2,0} & e_{2,1} & \dots & e_{2,N-n-2} & e_{2,N-n-1} \\ \vdots & \vdots & \ddots & \vdots & \vdots \\ e_{n-1,0} & e_{n-1,1} & \dots & e_{n-1,N-n-2} & e_{n-1,N-n-1} \\ e_{n,0} & e_{n,1} & & e_{n,N-n-2} & e_{n,N-n-1} \end{bmatrix}. \quad (20)$$

Assuming that error term \mathbf{E} is purely white noise with zero mean and variance σ^2 ,

$$E(e_i) = 0; E(e_i e_j) = \begin{cases} \sigma^2, & i = j \\ 0, & i \neq j \end{cases}. \quad (21)$$

Moreover, by focusing on \mathbf{Y} in wavelength domain,

$$Y_w = \sum_{p=0}^{N-1} y_p \cdot e^{-2\pi i \frac{p}{N} \frac{1}{w}} = A_w \cdot e^{i \cdot \theta_w}, \quad (22)$$

where i is the unit imaginary number with $i^2 = -1$; p represents spatial coordinate along the rail; w represents the wavelength related to frequency domain; and A_w and θ_w are the amplitude and phase of Y_w , respectively.

$$A_w = \text{Amp}(Y_w); \theta_w = \text{Ang}(Y_w) \quad (23)$$

Thereafter, we use A_w to define the FTG in wavelength domain (FWD) to describe the error property with respect to different wavelengths.

The spatial domain and wavelength domain for track geometry are similar to the time domain and frequency domain for time series, respectively. For a better understanding, we can imagine the EAF is similar to the standard deviation of False Track Geometry (FTG), while the FWD is similar to the Power Spectrum Density (PSD) of FTG.

4.2. Numerical experiment for FWD

The analytical analysis of the properties of A_w and θ_w is considerably challenging. Instead, in this study, numerical experiments were used to reveal the properties of A_w and θ_w . The numerical experiment is given in Appendix B.

Consider a case in which a 1-m-long chord is used to measure a 100-m rail section. The MCR(19) system with full configuration is used in this case. The probability distribution of A_w at different wavelengths based on the MCR(19) system is shown in Fig. 5. As shown, the magnitude gain of the long wavelength is large and as the wavelength decreases, the magnitude drops quickly until the wavelength is below 1.5 m, where the magnitude remains small with a slight fluctuation. The red-colored curve represents the average value at each wavelength.

The probability distributions of A_w at 100, 10, and 1 m are illustrated in Fig. 6. All of these probability distributions are similar to χ^2 -distribution. Both the average value and standard deviation are

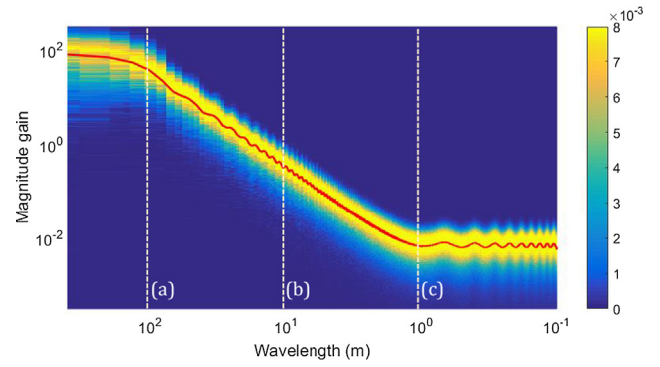


Fig. 5. Probability distribution of A_w at different wavelengths based on the MCR(19) system. The red curve represents the average value at each wavelength. The colors represent the probability distribution at each wavelength. The sections represented with white-dashed lines (a)–(c) are illustrated in Fig. 6. (For interpretation of the references to colour in this figure legend, the reader is referred to the web version of this article.)

larger for the long wavelengths than for the short wavelengths. The average and standard deviation of A_w at different wavelengths are illustrated in Fig. 7(a). Fig. 7(b) shows that the ratio between the average and the standard deviation of A_w is close to a constant 1.9. Owing to this constant ratio, we only need to present the average value at each wavelength.

$$\frac{E(A_w)}{\text{Std}(A_w)} = \text{constant} \approx 1.9. \quad (24)$$

For phase Y_w , θ_w obeys a uniform distribution in $[-\pi, \pi]$ for different MCR systems. Hereafter, the emphasis is on the property of A_w only.

4.3. FWD function

This section proposes a FWD function to describe A_w versus wavelength w . The A_w is currently divided into three parts: long, intermediate, and short wavelengths.

On the one hand, the magnitudes of wavelengths longer than 100 m tend to remain unchanged. A magnitude longer than the length of rail (100 m in this case) is denoted as A_{max} . The longer the rail length, the larger is A_{max} . On the other hand, for wavelengths shorter than 1.5 m, the magnitude remains low. We denote the magnitude lower than 1.5 times of the chord length (1.5 m in this case) as A_{min} . Numerically, A_{max} and A_{min} are estimated as follows:

$$A_{max} = \text{Max}_{w \geq l} (A_w) \quad (25)$$

$$A_{min} = \text{Mean}_{w < 1.5L} (A_w) \quad (26)$$

As for the intermediate wavelengths ($1.5L < w < l$), the magnitude is approximate to a linear function with dual logarithmic coordinate, indicating that the magnitude gain can be described as a power exponent function. Through power exponent fitting, the behavior of the intermediate wavelengths can be obtained. Two parameters are introduced, including coefficient A_{mid} and exponent P . A_{mid} determines the overall amplitude and P shows the steepness of the slope of the black line in Fig. 8.

As a result, the general form of the FWD function, denoted as $f_{wd}(w, \mathbf{M}_k, l, L)$, can be described as a piecewise function:

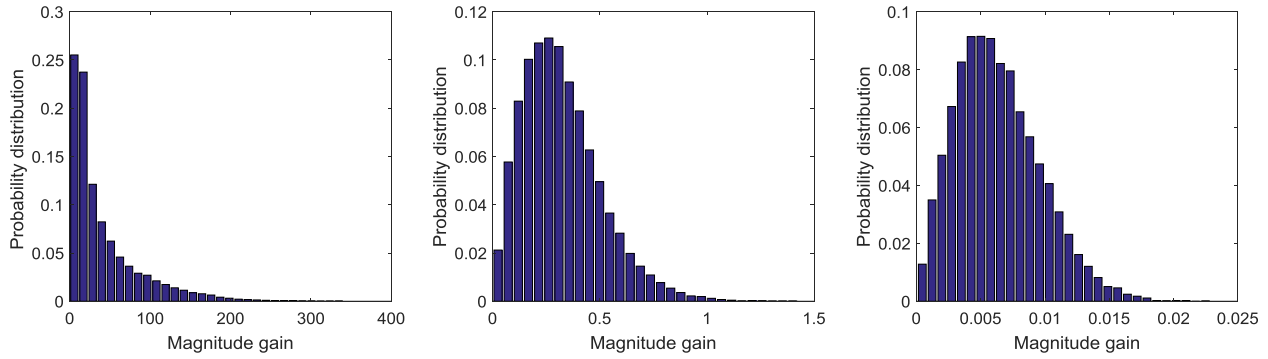


Fig. 6. Probability distribution of A_w at 100, 10, and 1 m wavelengths with respect to (a), (b), and (c) sections in Fig. 5.

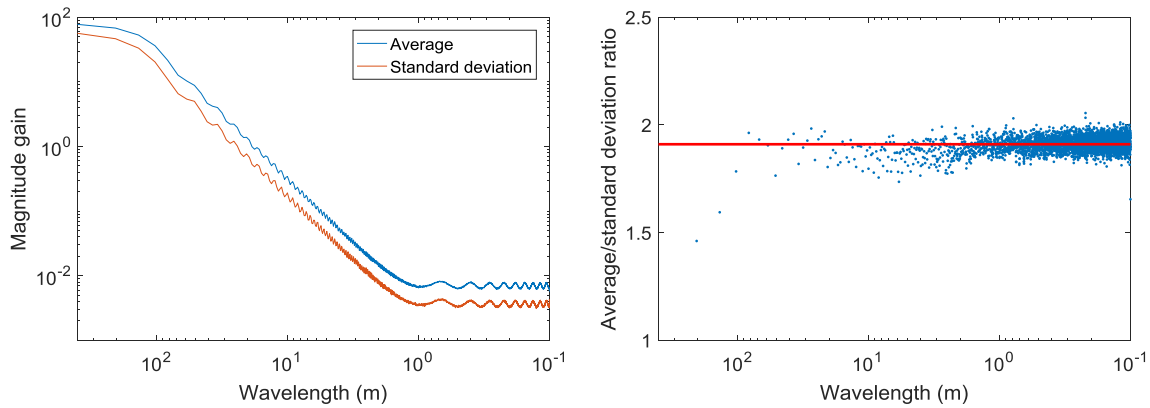


Fig. 7. Average and standard deviation of the magnitude gain. The average of the “average to standard deviation ratio” is approximately 1.9.

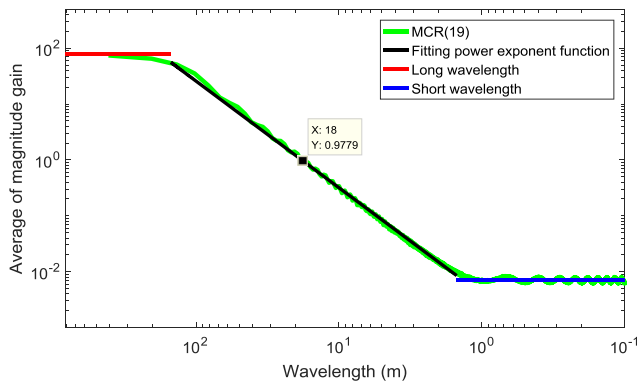


Fig. 8. FWD function f_{wd} for the MCR(19) system with full configuration. The chord and rail lengths are 1 and 100 m. Here, CW = 18 m.

$$f_{wd}(w, \mathbf{M}_k, l, L) = \begin{cases} A_{max}, & |w| \geq l \\ A_{mid} \cdot w^P, & |1.5L < w < l \\ A_{min}, & |w| \leq 1.5L \end{cases} \quad (27)$$

The four parameters in the brackets indicate that the FWD function is influenced only by w , \mathbf{M}_k , l , and L . A_{mid} and P are coefficients of a power exponent function for the intermediate wavelengths. In the case presented in Fig. 8, the FWD function is given as

$$f_{wd}(w, \mathbf{M}_k, 100, 1) = \begin{cases} 77.5, & |w| \geq 100 \\ 3.9 \times 10^{-3} \cdot w^{1.91}, & |1.5 < w < 100 \\ 7 \times 10^{-3}, & |w| \leq 1.5 \end{cases} \quad (28)$$

The FWD function given in Eq. (28) indicates that the FTG mainly contains a long-wavelength error term, such as the final

measurement error of 100-m wavelength, which is 77.5 times the amplified measurement error of the sensor. A longer wavelength contains larger error, and for wavelengths below 18 m, the expected magnitude of error is less than the measurement error of sensor. Especially for wavelength less than 1.5 m, the final measurement error is reduced to 7×10^{-3} of the measurement error of the sensor, indicating that the MCR systems with high order can be relatively efficient for measuring short-wavelength rail irregularity, such as corrugation.

Note that smaller values of A_{max} , A_{min} , and A_{mid} indicate a smaller FTG and better MCR system performance with a given length of chord and rail section to be measured.

4.4. CW

For an MCR system with given order and configuration, we define the CW as the wavelength where the FWD function is σ :

$$f_{wd}(W_c, \mathbf{M}_k, l, L) = \sigma, \quad (29)$$

where $\sigma = 1$ is the standard deviation of the white noise generated by the sensor. Note that CW is influenced by four factors: (1) the order, (2) configuration, (3) length of reference chord, and (4) length of rail to be measured.

CW is a critical value indicating that the wavelengths below W_c can achieve a measurement precision even better than the sensor precision. The measurement error accumulates for the wavelengths above W_c , while that of the wavelengths below W_c is reduced. CW can be considered as a representation of the measurement performance in the wavelength domain for a given MCR system. *The larger the CW, the better is the performance of the MCR system.*

5. Main factors for FWD

5.1. Main factors

This section analyzes the influence of the main factors on the performance of FWD functions for different MCR systems. The five parameters, A_{max} , A_{min} , A_{mid} , P , and CW are used as the main tools to quantify and describe the error property of different MCR systems in the wavelength domain.

The following three major factors are considered:

Order of the MCR system. In general, a higher order leads to higher measurement precision and smaller MMW. The topic of concern is the quantification of the relationship between the order and measurement precision. This is discussed in Section 5.2.

Configuration of the MCR system. Sparse configuration can reduce the total cost as less sensors are used; however, at the same time, the measurement precision may be lower. Here, the exact influence of different configurations on the FWD function must be determined. This is discussed in Section 5.3.

Length of rail to be measured. Measurement error accumulates with the increasing length of rail. For this, the performance of the measurement error in the wavelength domain must be analyzed; this analysis is presented in Section 5.4.

5.2. Order of MCR system

This section analyzes the FWD function with respect to the order of the MCR system. In this section, the full configuration of MCR systems with orders 1–19 are used as a case study. The FWD functions of different orders are estimated through numerical

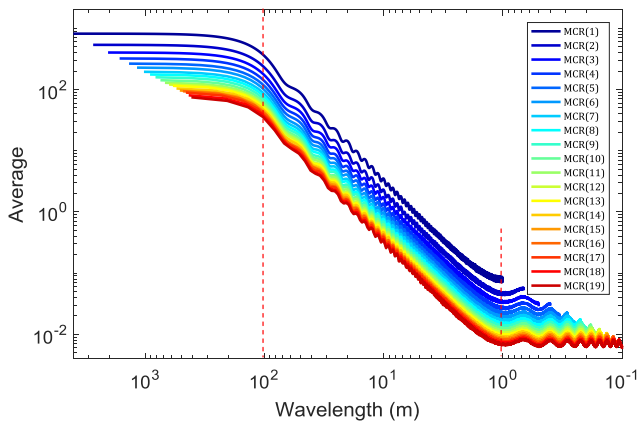


Fig. 9. FWD of an MCR(n) system with full configuration.

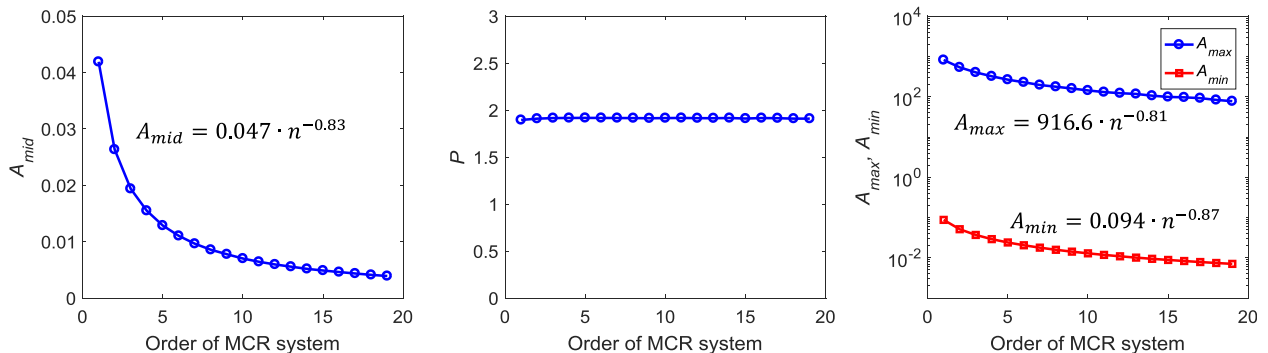


Fig. 10. A_{max} , A_{min} , A_{mid} , and P versus the order of the MCR system. The data is provided in Table A1.

experiments given in Section 5.2, as presented in Fig. 9. The parameters of FWD function $f_{wd}(w, \mathbf{M}_k, l, L)$, including A_{max} , A_{min} , A_{mid} , and P , for each curve in Fig. 9 are estimated, and the results are illustrated in Fig. 10.

The following results are summarized from Figs. 9–11:

The FWD function of an MCR system with higher order contains smaller wavelength components, which are related to the MMW of the MCR system.

The FWD function over the whole wavelength domain decreases with the increasing order of the MCR system. Coefficients A_{max} , A_{min} , and A_{mid} of the FWD function decrease with speed as

$$\begin{cases} A_{max} = 916.6 \cdot n^{-0.81} \\ A_{min} = 0.094 \cdot n^{-0.87} \\ A_{mid} = 0.047 \cdot n^{-0.83} \end{cases}, \quad (30)$$

where n is order of the MCR system.

Parameter P , namely the slope of each curve in Fig. 9, remains approximately 1.91 for different orders of the MCR system.

As a result, the $f_{wd}(w, \mathbf{M}_n, 100, 1)$ can be described as

$$f_{wd}(w, \mathbf{M}_n, 100, 1) = \begin{cases} 916.6 \cdot n^{-0.81}, & |w| \geq 100 \\ 0.0466 \cdot n^{-0.83} \cdot w^{1.91}, & |1.5 < w| < 100, \\ 0.094 \cdot n^{-0.87}, & |w| \leq 1.5 \end{cases} \quad (31)$$

where subscript n in \mathbf{M}_n indicates that the MCR systems are specified by full configuration.

With the increasing system order, the MMW decreases as $MMW = 2/(n + 1)$ and CW shows an increasing trend, that is, $CW = 2.79n^{0.59} + 2.54$. Both the trends of MMW and CW indicate that a higher order results in better performance of the MCR system in the wavelength domain.

5.3. Configuration of MCR system

This section analyzes the FWD function regarding the influence of different configurations of an MCR system. A series of MCR(16, 1) and MCR(16, 2) systems were used in a case study.

The MCR(16, 1) system possesses eight configurations when considering the symmetric distribution pairs, e.g., configurations of $k = 1$ and 16 are symmetric. Fig. 12 shows the eight FWDs of MCR(16) system with sparse configuration for $k = \{1\}, \{2\}, \dots, \{8\}$. The sensor was determined to move from the edge to the middle of the reference chord, and the whole wavelength range above

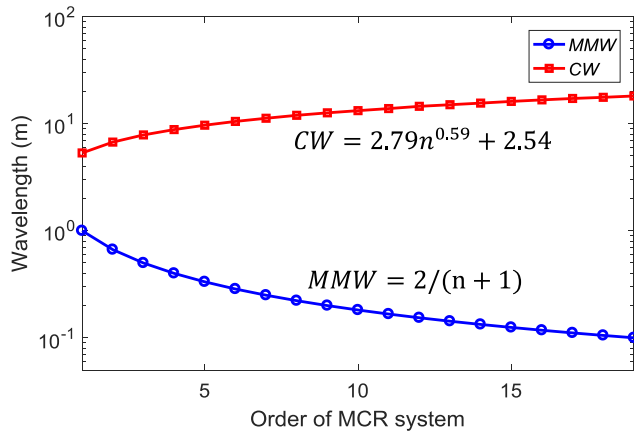


Fig. 11. MMW and CW versus the order of the MCR system. The data is provided in Table A1.

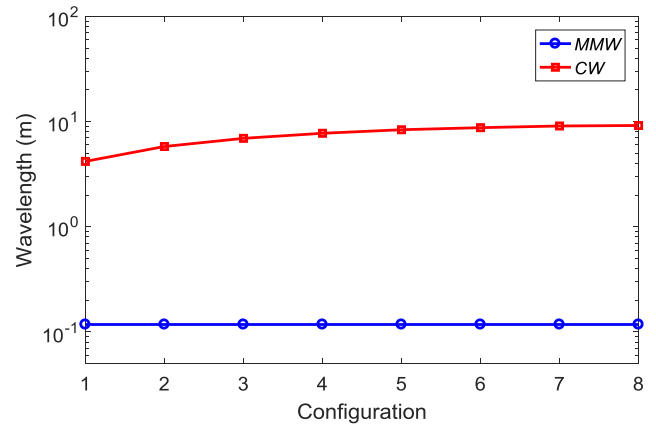


Fig. 14. MMW and CW for different configurations of MCR system. The data is provided in Table A2.

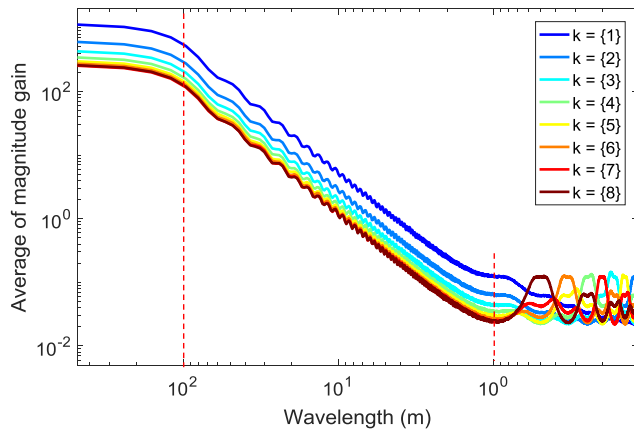


Fig. 12. FWD of MCR(16) system with sparse configuration. MCR(16, 1) system with $k = \{1, \{2\}, \dots, \{8\}$.

1 m shows a decreasing trend, indicating the reduction in the final measurement error. The corresponding parameters A_{max} , A_{min} , A_{mid} , and P are presented in Fig. 13. Both A_{max} and A_{mid} show a decreasing trend, while P remains approximately 1.91. Note that for the wavelength below 1.5 m, the FWDs show large fluctuations although A_{min} shares a similar value of approximately $4.8E-02$. This indicates that sparse configurations of MCR(n , 1) systems may have significant influence on short wavelength components of FWD.

The MMW and CW of MCR(16, 1) systems are presented in Fig. 14. As shown, the MMW is fixed at $2/(16 + 1) \approx 0.12$ m. The CWs of the eight configurations of MCR(16, 1) show an increasing trend as the sensor moves toward the middle of chord.

Based on all the above-mentioned results, we can draw the following conclusions.

The EPs around the middle of the chord seem more valuable than those close to the edges with decreases in A_{max} and A_{mid} and increase in CW.

The configurations have a significant influence on FTG for the short wavelengths below 1.5 m.

5.4. Measurement length of rail

This section presents the analysis of the FWD function with respect to the influence of the length of rail to be measured. The MCR(9) systems with full and sparse configurations specified by $k = \{1, 5\}$ are used as a case study. The considered rail length varies from 20 to 200 m, with step of 10 m. The FWDs for different rail lengths are presented in Fig. 15, with parameters A_{max} , A_{min} , A_{mid} , and P given in Figs. 16 and 17 presents MMW and CW.

The following results are summarized based on data Figs. 15–17. Some insights on those results are explained in the Section 7.

With the increase in rail length, A_{max} increases for both full and sparse configurations, while A_{min} and A_{mid} decrease.

$$\begin{cases} A_{max} = 0.342 \cdot l^{1.5} \\ A_{min} = 0.734 \cdot l^{-0.647} \\ A_{mid} = 0.104 \cdot l^{-0.562} \end{cases} \quad (32)$$

Parameter P approximates to 1.91 with the increase in the measured rail length. P is slightly lower than 1.91 when rail length

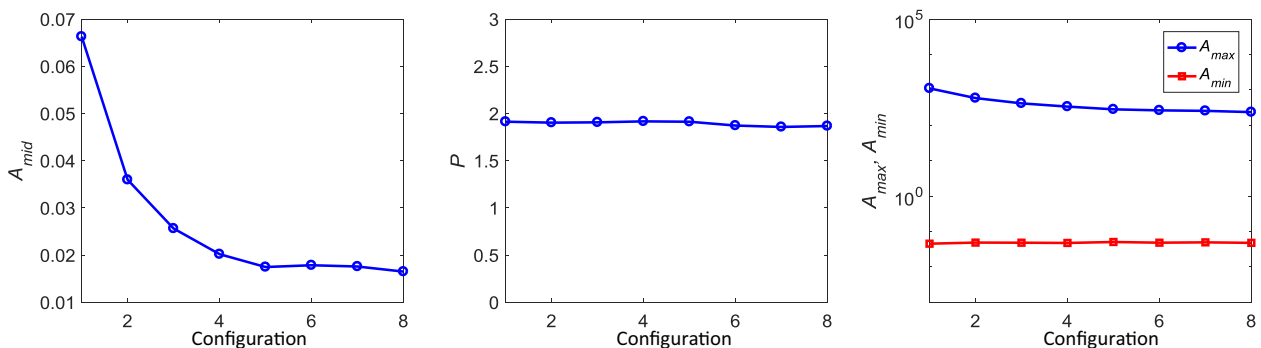


Fig. 13. A_{max} , A_{min} , A_{mid} , and P for sparse configurations $k = \{1, \{2\}, \dots, \{8\}$ of MCR(16, 1) system. The data is provided in Table A2.

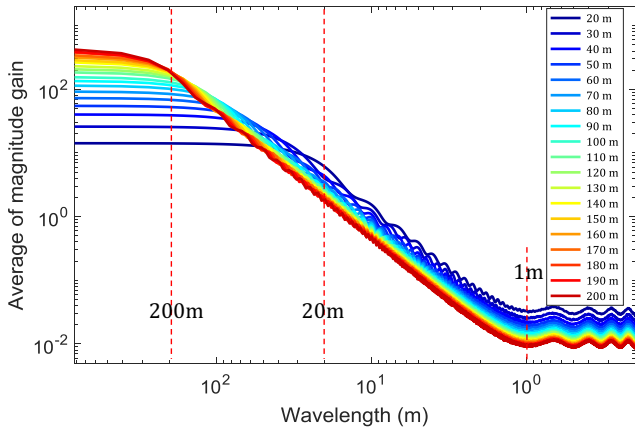


Fig. 15. FWD of the MCR(9) system with full configuration, considering rail length of 20–200 m at 10-m steps.

is 20 m. The decrease of P results from the unstable fitting performance on a small wavelength range of [1.5, 20].

$f_{wd}(w, \mathbf{M}_n, l, 1)$ can be described as

$$f_{wd}(w, \mathbf{M}_n, l, 1) = \begin{cases} 0.342 \cdot l^{1.5}, & |w| \geq l \\ 0.104 \cdot l^{-0.562} \cdot w^{1.91}, & |1.5 < w < l, \\ 0.734 \cdot l^{-0.647}, & |w| \leq 1.5 \end{cases} \quad (33)$$

where subscript n in \mathbf{M}_n indicates that the MCR systems are specified by full configuration.

The MMW retains a value of $2/(9 + 1) = 0.2$ and CW shows an increasing trend, which can be described as $W_c = 1.26 \cdot l^{0.4} + 4.672$. This indicates that a longer rail length results in a larger FTG for long wavelengths but facilitates the short wavelength range (below $1.5L$) in becoming more accurate.

6. Discussion

The use of a high-order MCR system will greatly improve the measurement precision because high-order MCR system requires more sensors and a high sampling frequency. Note that by simply improving the sampling frequency for low-order MCR systems, the system performance can be significantly enhanced similar to that when using higher-order MCR systems. However, one major advantage of using high-order MCR systems is that they can achieve smaller MMW; this could be essential when dealing with

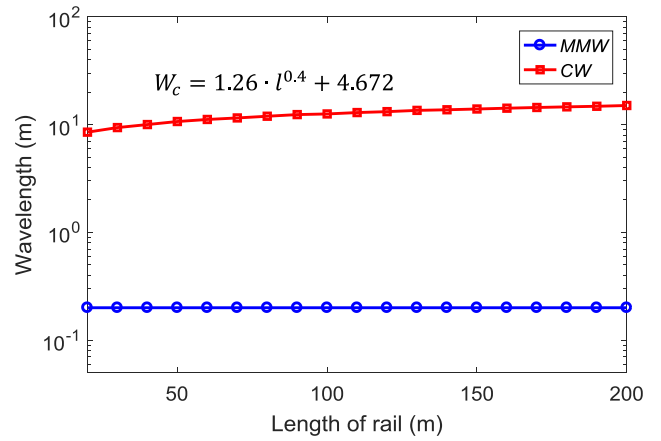


Fig. 17. MMW and CW for different rail lengths, as listed in Table A3.

short wavelength components in rail irregularity, such as rail corrugation.

To make a fair comparison between high- and low-order MCR systems with high sampling frequencies, an MCR(1) system is taken as a reference. In this system, only one sensor is used and the sampling interval is $1/(1 + 1) = 0.5$ m. Compared to an MCR(n) system with full configuration, in which n sensors are used and the sampling interval is $1/(n + 1)$, the equivalent parameters \hat{A}_{max} , \hat{A}_{min} , and \hat{A}_{mid} for MCR(1) system with n times the repeated measurements, each with sampling intervals of $1/(n + 1)$, are given as

$$\hat{A}_{max}(n) = \frac{A_{max}(1)}{\sqrt{n} \cdot \sqrt{\frac{n+1}{2}}}; \hat{A}_{min}(n) = \frac{A_{min}(1)}{\sqrt{n} \cdot \sqrt{\frac{n+1}{2}}}; \hat{A}_{mid}(n) = \frac{A_{mid}(1)}{\sqrt{n} \cdot \sqrt{\frac{n+1}{2}}}, \quad (34)$$

where the number in the brackets refers to the order; \hat{A}_{max} , \hat{A}_{min} , and \hat{A}_{mid} are the equivalent parameters with respect to A_{max} , A_{min} , and A_{mid} , respectively. The comparisons between $\hat{A}_i(n)$ and $A_i(n)$ are illustrated in Fig. 18. As shown, parameters A_{max} and A_{mid} of the MCR(n) system are slightly larger than the equivalent parameters \hat{A}_{max} and \hat{A}_{mid} , respectively, indicating that the performance in wavelengths above $1.5L$ is not as good as that of the MCR(1) system with high-frequency sampling. For the short wavelength below $1.5L$, the difference can be ignored. From this point of view, we can conclude that the high-order MCR system can achieve a significant improvement in short wavelengths by sacrificing a small amount of precision in long wavelengths compared to the low-order MCR system with high frequency sampling.

Furthermore, in the spatial domain, we found that the magnitude of FTG increases with rail length, indicating that error

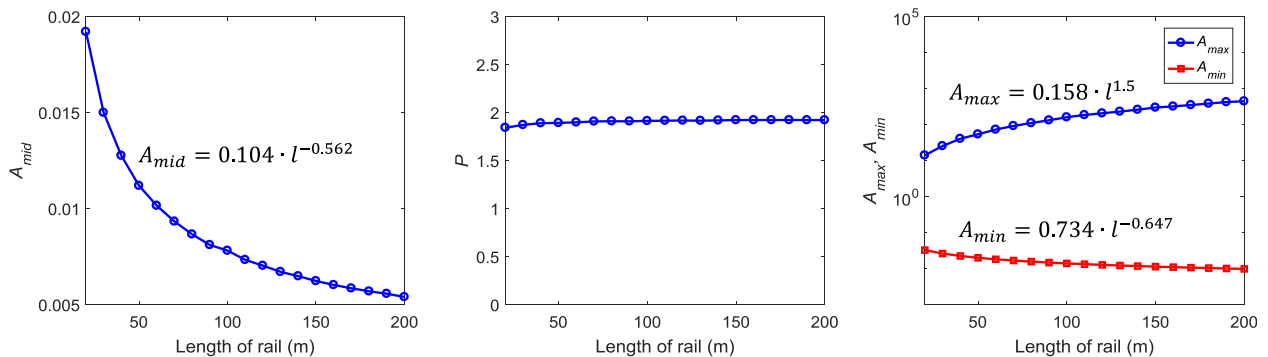


Fig. 16. A_{max} , A_{min} , A_{mid} , and P for the MCR(9) system with full configuration, considering rail lengths of 20–200 m. The data is provided in Table A3.

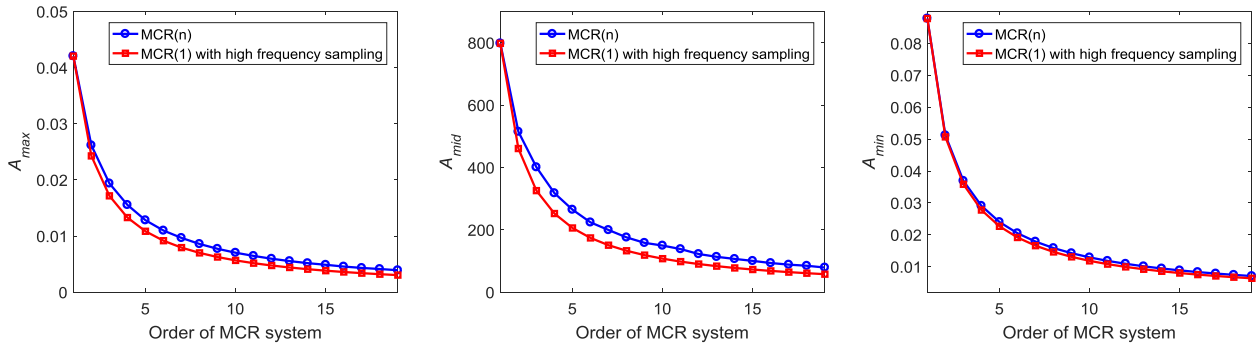


Fig. 18. Comparison of parameters A_{max} , A_{min} , and A_{mid} between high-order MCR(n) and MCR(1) systems with high frequency sampling.

accumulates gradually with rail length. However, in the wavelength domain, only the magnitude of long wavelength components increases rapidly, while that of the short wavelength components get more accurate with longer rail length. Actually, this phenomenon is quite similar to the inertial drift phenomenon of inertial navigation system [14], where the error grows with time (if no additional information is used to correct the error). Both MCR systems and inertial navigation system are relative measurement techniques, which measure the microcosmic information to restore the macroscopic structure. In this process, the error accumulates gradually with distance or time.

7. Conclusion

This study analyzed the performance of an MCR system in the wavelength domain according to two aspects: (1) the TF and (2) FWD. Numerical simulations were used throughout this study.

The MMWs were analyzed according to the performance of the TFs of MCR systems with different orders. The simulation results are consistent with the theoretical values of MMW denoted as $2/(n+1)$.

To analyze FWD, a numerical experiment based on Fourier transform was proposed, through which the FWD curve for a given MCR system could be obtained. Furthermore, to describe the FWD curve, the FWD function was defined using a piecewise function including two linear functions and a power exponent function. The FWD function comprises four parameters, A_{max} , A_{min} , A_{mid} , and P , which are of utmost importance for the description of the FWD curve. Particularly, the CW was proposed to quantify the performance of the MCR system. A larger CW indicates a better performance of an MCR system.

Furthermore, the influence of the major factors on the performance of FWD for different MCR systems was analyzed. Three major factors, that is, the order, configuration, and length of the rail were also measured. The quantification of the performance of FWD was based on parameters A_{max} , A_{min} , A_{mid} , and P of FWD functions as well as MMW and CW. The main results are as follows:

A higher order results in a better performance of the MCR system in the wavelength domain, smaller MMW, and larger CW. Coefficients A_{max} , A_{min} , and A_{mid} of the FWD function are proportional to $n^{-0.81}$, $n^{-0.87}$, and $n^{-0.83}$, respectively.

The magnitude of FTG increases rapidly with the increase of the wavelength with speed $w^{1.91}$.

For the same ordered MCR systems, the MMW remains constant as $2/(n+1)$. The sparse configurations have a significant influence on the FTG for the short wavelengths below 1.5 m.

When measuring longer lengths of rail sections, the magnitude of FTG for long wavelengths increases in speed proportional to

$l^{1.5}$. However, coefficients A_{min} and A_{mid} decrease with speeds $l^{-0.562}$ and $l^{-0.647}$, respectively.

CW increases with the increasing order of the MCR system or with the increasing length of rail to be measured.

Acknowledgements

The present work was supported by the National Natural Science Foundation of China (51425804, 51608459 and 51378439) and the United Fund for Key Projects of China's High-Speed Railway (U1334203 and U1234201). The authors Yuan Wang (No. 201707000036) and Huiyue Tang (No. 201707000037) were financially supported by the China Scholarship Council CSC. Dr. Xiang Liu was funded by the US Federal Railroad Administration at the time of writing this paper. However, the authors are solely responsible for all views and analyses in this research.

Appendix A. Simulation of measurement process

The steps for the simulation of measurement process are as follows.

- (1) **Initialization:** An irregular rail with length l and track-geometry irregularity waveform is generated based on the sixth-grade track-irregularity of the U.S. PSDs. The rail is discretized by a sufficiently small interval (1 mm in this study), and a reference chord (line \overline{AB} in Fig. 2) with length L is considered. m sensors are mounted on the EPs of the chord with the layout specified by sequence $k = \{k_i | i = 0, 1, \dots, m; k_i \in N^+ \cap [1, n]\}$. Then, the precision of the sensor is specified, assuming white noise as $E(e) = 0; E(e^2) = \sigma^2$.
- (2) **Move the chord on the rail:** one end of the reference chord (point A in Fig. 2) is placed on the rail. The other end (point B in Fig. 2) is determined by searching for the nearest point on the rail with a fixed distance L .
- (3) **Measure the chord versine:** The i th sensor is iterated at the k_i th EP, the nearest point is searched on the rail at the normal direction, the distance between the EP and searched point is measured, and the versine values of the measured chord are recorded.
- (4) **Move on:** End A of the reference chord is moved to the next point on the rail with a given sampling interval ΔL ; the steps are repeated from Step (2) until the end of the rail is reached.
- (5) **Output:** after moving the chord, the measured chord versine values are output in a matrix form, with each row containing the readouts from one sensor, as shown in Eq. (9).

$$H = \begin{bmatrix} h_{k_1,0} & \cdots & h_{k_1,N-n-1} \\ h_{k_2,0} & \cdots & h_{k_2,N-n-1} \\ \vdots & \ddots & \vdots \\ h_{k_m,0} & \cdots & h_{k_m,N-n-1} \end{bmatrix}, \tag{9}$$

where subscript i of $h_{i,j}$ indicates the serial number of sensor.

Appendix B. Numerical experiment for FWD

The steps of the numerical experiment can be described as follows.

- (1) **Initialization:** Specify chord length L , rail length l to be measured, MCR(n, m) system with order n , and configuration of the MCR(n, m) system according to sequence $k = \{k_i | i = 0, 1, \dots, m; k_i \in N^+ \cap [1, n]\}$;
- (2) **Generate the sensor error matrix E :** Generate sensor error matrix E by using white noise such that $E(e) = 0; E(e^2) = \sigma^2 = 1$.
- (3) **Calculate y :** for a given sensor error matrix E , calculate FTG y according to Eq.19.
- (4) **Calculate Y, A_w , and θ_w :** for a given FTG y , calculate FWD Y according to Eq. (22), and then amplitude A_w as well as phase θ_w are obtained according to Eq. (23).
- (5) **Steps (2–4) are repeated sufficient times:** Repeat Steps 2–4 sufficient times; each time, sensor error matrix E is newly generated according to Step 1. Here, *sufficient times* implies that there should be *sufficient* samples of y , and thus the properties of A_w and θ_w can be determined with statistical significance.
- (6) **Estimate the distribution of A_w and θ_w :** Estimate the distribution of A_w and θ_w based on the samples obtained in Step (5).

Appendix C. Influence of order, configuration, and length of rail.

Table A1
 $A_{max}, A_{min}, A_{mid}, P, MMW$, and CW versus different orders of MCR systems with full configurations.

Order n	A_{mid}	P	A_{max}	A_{min}	MMW (m)	CW (m)
1	4.19E-02	1.896	817.2	8.76E-02	1.00	5.33
2	2.63E-02	1.909	536.8	5.13E-02	0.67	6.73
3	1.94E-02	1.916	402.4	3.70E-02	0.50	7.85
4	1.55E-02	1.917	321.8	2.91E-02	0.40	8.81
5	1.29E-02	1.918	265.4	2.41E-02	0.33	9.68
6	1.10E-02	1.917	228.7	2.05E-02	0.29	10.51
7	9.64E-03	1.916	195.6	1.79E-02	0.25	11.24
8	8.57E-03	1.916	177.2	1.58E-02	0.22	11.98
9	7.78E-03	1.914	160.0	1.42E-02	0.20	12.64
10	7.02E-03	1.916	143.4	1.29E-02	0.18	13.25
11	6.44E-03	1.917	130.6	1.18E-02	0.17	13.85
12	5.97E-03	1.915	122.6	1.09E-02	0.15	14.54
13	5.57E-03	1.914	117.3	1.01E-02	0.14	15.05
14	5.18E-03	1.916	106.2	9.45E-03	0.13	15.58
15	4.89E-03	1.911	98.9	8.86E-03	0.13	16.16
16	4.62E-03	1.916	96.6	8.33E-03	0.12	16.70
17	4.37E-03	1.914	92.3	7.86E-03	0.11	17.21
18	4.12E-03	1.910	83.3	7.45E-03	0.11	17.64
19	3.92E-03	1.910	77.5	7.08E-03	0.10	18.16

Table A2
 $A_{max}, A_{min}, A_{mid}, P, MMW$, and CW for sparse configurations $k = \{1\}, \{2\}, \dots, \{8\}$ of MCR (16, 1) system.

Configuration k	A_{mid}	P	A_{max}	A_{min}	MMW (m)	CW (m)
{1}	6.63E-02	1.913	1105.1	4.52E-02	0.12	4.19
{2}	3.60E-02	1.903	587.4	4.85E-02	0.12	5.80
{3}	2.56E-02	1.906	416.3	4.81E-02	0.12	6.93
{4}	2.02E-02	1.916	337.4	4.73E-02	0.12	7.75
{5}	1.75E-02	1.913	282.3	5.04E-02	0.12	8.37
{6}	1.78E-02	1.872	264.0	4.82E-02	0.12	8.76
{7}	1.76E-02	1.857	255.6	4.92E-02	0.12	9.09
{8}	1.65E-02	1.867	235.5	4.77E-02	0.12	9.19

Table A3
 $A_{max}, A_{min}, A_{mid}, P, MMW$, and CW for full configurations of MCR(9) system considering rail lengths of 20–200 m.

Length of rail (m)	A_{mid}	P	A_{max}	A_{min}	MMW (m)	CW (m)
20	2.09E-02	1.761	14.2	3.33E-02	0.20	8.95
30	1.54E-02	1.846	26.0	2.67E-02	0.20	9.58
40	1.27E-02	1.885	40.3	2.29E-02	0.20	10.13
50	1.12E-02	1.897	55.1	2.04E-02	0.20	10.62
60	1.01E-02	1.907	73.1	1.85E-02	0.20	11.08
70	9.26E-03	1.913	92.4	1.71E-02	0.20	11.51
80	8.66E-03	1.916	114.9	1.60E-02	0.20	11.96
90	8.14E-03	1.914	136.2	1.50E-02	0.20	12.35
100	7.75E-03	1.915	156.4	1.42E-02	0.20	12.65
110	7.42E-03	1.914	186.3	1.36E-02	0.20	12.96
120	7.08E-03	1.914	209.2	1.30E-02	0.20	13.29
130	6.73E-03	1.919	235.2	1.25E-02	0.20	13.50
140	6.51E-03	1.917	270.4	1.20E-02	0.20	13.78
150	6.29E-03	1.918	293.2	1.16E-02	0.20	14.11
160	6.10E-03	1.917	326.0	1.12E-02	0.20	14.29
170	5.89E-03	1.921	351.7	1.09E-02	0.20	14.52
180	5.71E-03	1.921	392.5	1.06E-02	0.20	14.70
190	5.52E-03	1.920	401.9	1.03E-02	0.20	14.85
200	5.40E-03	1.919	438.1	1.00E-02	0.20	15.17

References

- [1] W. Ping, W. Yuan, T. Huiyue, et al., Error theory of chord-based measurement system regarding track geometry and improvement by high frequency sampling, *Measurement* 115 (2) (2018) 204–216.
- [2] A. Haigermoser, B. Luber, J. Rauh, G. Gräfe, Road and track irregularities: measurement, assessment and simulation, *Vehicle Syst. Dyn.* 53 (7) (2015) 878–957.
- [3] Jens Nielsen, Eric Berggren, Overview of methods for measurement of track irregularities important for ground-borne vibration, *Rivas Chalmers WP2 Deliverable* (2013) D2.5.
- [4] Akiyoshi Yoshimura, Study on theoretical foundations to restoring an original waveform of track irregularity and its application, *Proc. Jpn. Soc. Civil Eng.* 377 (1987) 117–126.
- [5] A. Yoshimura, Y. Okumura, T. Anami, M. Kamiyama, A new method of repairing railway track irregularity using the restored waveform and its application, *Quart. Report of RTRI (Railway Technical Research Institute) (Japan)* 38 (1) (1997) 13–18.
- [6] M. Kamiyama, A. Furukawa, A. Yoshimura, Theory and practice of optimum correction using restored track irregularity waveform, *Quarter. Report RTRI* 40 (2) (1999) 117–122.
- [7] S. Wang, Y. Xu, Y. Zhou, et al., Study of Rail Surface Irregularity Detection Based on Asymmetrical Chord Offset Method, *Third International Conference on Mechanic Automation and Control Engineering*, 2012, pp. 829–832.
- [8] K.U. Wolter, Reconstruction of original signals from relative measurement: EP, EP 1543439 A1 (2005).
- [9] X.J. Mao, H.F. Li, Y.D. Xu, A new method for detecting rail short wave irregularity, *Appl. Mech. Mater.* 361–363 (2013) 1640–1644.
- [10] A. Ben-Israel, T.N.E. Greville, *Generalized Inverses: Theory and Applications*, Wiley, 1974.
- [11] J.J. Zhao, Track irregularity simulation of rubber-tired light rail transit, *Appl. Mech. Mater.* 427–429 (2013) 3–6.
- [12] P.S.I. Snowball, Spectral analysis of signals, *Leber Magen Darm* 13 (2) (2005) 57–63.
- [13] D. Percival, A. Walden, *Spectral Analysis for Physical Applications*, Cambridge University Press, 1998.
- [14] D.E. Adams, *Introduction to Inertial Navigation*, *J. Navig.* 9 (3) (1956) 11.